

Identifying the rotation rate and the presence of dynamic weather on extrasolar Earth-like planets from photometric observations.

E. Pallé¹, Eric B. Ford², S. Seager³, P. Montañés-Rodríguez¹, M. Vazquez¹

Instituto de Astrofísica de Canarias, La Laguna, E38200, Spain.

epalle@iac.es, pmr@iac.es, mva@iac.es

Department of Astronomy, University of Florida, 211 Bryant Space Science Center, PO Box 112055 Gainesville, FL, 32611-2055, USA

eford@astro.ufl.edu

EAPS, Massachusetts Institute of Technology, Cambridge, MA02139-4307, USA

seager@MIT.EDU

ABSTRACT

With the recent discoveries of hundreds of extrasolar planets, the search for planets like Earth and life in the universe, is quickly gaining momentum. In the future, large space observatories could directly detect the light scattered from rocky planets, but they would not be able to spatially resolve a planet's surface. Using reflectance models and real cloud data from satellite observations, here we show that, despite Earth's dynamic weather patterns, the light scattered by the Earth to a hypothetical distant observer as a function of time contains sufficient information to accurately measure Earth's rotation period. This is because ocean currents and continents result in relatively stable averaged global cloud patterns. The accuracy of these measurements will vary with the viewing geometry and other observational constraints. If the rotation period can be measured with accuracy, data spanning several months could be coherently combined to obtain spectroscopic information about individual regions of the planetary surface. Moreover, deviations from a periodic signal can be used to infer the presence of relatively short-live structures in its atmosphere (i.e., clouds). This could provide a useful technique for recognizing exoplanets that have active weather systems, changing on a timescale comparable to their rotation. Such variability is likely to be related to the atmospheric temperature and pressure being near a phase transition and could support the possibility of liquid water on the planet's surface.

Subject headings: exoplanets, Earth, albedo, earthshine, rotation, astrobiology

1. Introduction

Over the past two decades, more than 240 planets have been discovered orbiting stars other than the Sun. To date all planets discovered around main sequence stars are significantly more massive than the rocky planets of the solar system. Radial velocity surveys, however, are starting to detect rocky planet candidates below 10 Earth masses (Rivera et al., 2006; Udry et al, 2007) and, for the coming decades, ambitious space missions are being proposed that would be able to detect nearby planets with physical properties similar to Earth (see, e.g., Lindensmith , 2003; Kaltenegger, 2005; Fridlund, 2004; Cash, 2005; Schneider et al, 2006).

Among other important physical properties, the identification of the rotation rate of an exoplanet with relatively high accuracy will be important for several reasons (Laskar and Correia, 2004). First, measuring the rotation rate can help to understand the formation mechanisms and dynamical evolution of extrasolar planetary systems (Agnor et al., 1999; Chambers, 2001; Goldreich et al., 2004). For example, are planetary rotation periods smoothly varying as a function of the planet mass and semi-major axis, as would be expected if the planet’s angular momentum is dominated by the gradual accretion of small planetesimals? Or are planet’s rotation periods essentially uncorrelated with their mass and orbital properties, as would be the case if the planet’s angular momentum is dominated by the late accretion of a few large impactors? The rotation periods of a sample of planets could be directly compared to numerical simulations of planetary formation that track the spin evolution of planets, to probe the late stages of planetary accretion (Schlichting and Sari, 2007).

A precise determination of the rotation rate can also help improve our analysis of future direct detections of exoplanets, including photometric, spectroscopic, and potentially polarimetric observations (Gaidos and Williams, 2004; Tinetti et al, 2006; Montañés-Rodríguez et al., 2005; Stam et al, 2006; Williams and Gaidos, 2007). For practical viewing geometries, most of the light scattered by an Earth-like planet comes from a small portion of the planet, and contains information about weather patterns, surface features, i.e. lands and oceans. While even the most ambitious space telescopes will not be able to spatially resolve the surface of an extrasolar planet, the temporal variability contains information about regional surface and/or atmospheric features, possibly including localized biomarkers (Ford et al., 2003; Seager et al, 2005; Montañés-Rodríguez et al., 2006). Determining the planet rotation period is necessary in order to know the rotational phase for a time series of observations.

The precision with which the rotation period can be measured determines the time span of observations that can be coherently averaged.

We will see in this paper how the deviations from a periodic photometric signal can help to identify active weather on an exoplanet. This could prove a useful technique for recognizing exoplanets that have weather systems with inhomogeneous cloud patterns.

Finally, the observations of our solar system bodies suggest that the presence of a planetary magnetic field, generated by dynamo processes, is mainly a function of two parameters: its composition (mass) and the rotation speed (Vallee, 1998; Russell, 2006). If the planet mass is known, a fast rotation speed of the planet could suggest the presence of a significant magnetic field. One must note however that there will be a large list of caveats to this possibility, given our current understanding of dynamos and planetary evolution (Bushby and Mason, 2004; Grießmeier, 2007).

In this paper we have determined the changes in photometric albedo that we would see if Earth was observed as an extrasolar planet. First, we perform an accurate and realistic simulation of the flux changes in reflected light from the planet’s surface and atmosphere. Second, we perform a periodicity analysis to determine under what conditions the rotation rate can be determined. Third, we explore how the accuracy and precision of the measured rotation rate depend on four variables: the temporal resolution of observations (i.e., exposure time), the total duration of observations, the signal-to-noise ratio, and the viewing geometry. We also discuss the role of clouds in altering the reflected light flux from Earth, and how to detect them in an exoplanet’s atmosphere. Finally, we discuss the implications for the design of future space missions to characterize extrasolar planets via direct detection.

2. Methods

2.1. Planet Light Scattering Model

The albedo of each surface element, a , depends on the surface type, cloud and snow/ice cover and solar zenith angle. Further, there is an anisotropic factor, L , that gives the angular distribution of the reflected radiation and depends upon the reflected zenith angle and azimuth. The anisotropy function, also known as bidirectional reflectance function (BDRF), generally depends on surface type, cloud cover, zenith angle and relative azimuth of the Sun. L is defined so that it is unity for a Lambert surface (Pallé et al, 2003). In modeling the reflectance properties, a and L , of the Earth, we used scene models based on the Earth Radiation Budget Experiment (ERBE) observations (Suttles et al., 1988), defined as the mean over the broad shortwave interval from 200 to 4000 nm . The parameters a and

L are tabulated for twelve model scenes.

The model of the Earth uses daily satellite observations of total cloud amount at each surface location from the International Satellite Cloud Climatology Project (ISCCP) as input (Rossow et al., 1996). Four cloudiness levels (0-5%, 5-50%, 50-95% and 95-100%), are considered for each of the 12 different ERBE scenes. For the snow/ice cover, we used simulations from the Canadian Center for Climate Modeling and Analysis (CCCM II). The model has already been validated by observations of Earthshine (Pallé et al, 2003).

Our model allows us to simulate the Earth’s reflectance observed from any viewing geometry. For example, looking at the exoplanet (our modeled Earth) always from the north pole or along the ecliptic. In the context of observing extrasolar planets, this is similar to fixing the orbital inclination of the orbit with respect to the observation point. Thus, the Earth’s reflectance in the direction of β , where β is defined as the angle between the Sun-Earth and Earth-Observer vectors, can be expressed as

$$p_e f_e(\beta) = \frac{1}{\pi R_e^2} \int_{(\hat{R} \cdot \hat{S}, \hat{R} \cdot \hat{M}) \geq 0} d^2 R(\hat{R} \cdot \hat{S}) a(\hat{R} \cdot \hat{M}) L, \quad (1)$$

where \hat{R} is the unit vector pointing from the center of the Earth to a patch of Earth’s surface, \hat{S} is the unit vector pointing from the Earth to the star, and \hat{M} is the unit vector pointing from the Earth toward the observer. The integral is over all of the Earth’s surface elements for which the sun is above the horizon (i.e., $\hat{R} \cdot \hat{S}$) and the surface element is visible from the observer’s perspective (i.e., $\hat{R} \cdot \hat{M} \geq 0$). Here R_e is the radius of the Earth, p_e is the geometrical albedo of the Earth, and $f_e(\beta)$ is the Earth’s phase function (defined such that $f_e(0) = 1$).

The total reflected flux in a given direction, β , can be calculate using

$$F_e(\beta) = S \pi R_e^2 p_e f_e(\beta), \quad (2)$$

where S is the solar flux at the top of the Earth’s atmosphere ($1370W/m^2$). There is a systematic variation of $p_e f_e(\beta)$ throughout the Earth’s orbital period (sidereal year), and fluctuations of $p_e f_e(\beta)$ about its systematic behavior are caused by varying terrestrial conditions, including weather and seasons (Pallé et al, 2004).

Comparing F_e to the flux of sunlight for the same observer, yields contrast ratios of order 10^{-10} . This presents the main challenge in directly detecting an Earth-like planet. In comparison, the amplitude of the diurnal cycle of the Earth observed in our broadband (200 – 4000nm) simulations (Figure 1) is of the order of 0.5×10^{-11} , but varies greatly depending on wavelength.

At present, broadband coronagraphic experiments are able to reach contrasts of 10^{-3} only (Mawet et al., 2006). However, advances in the development of coronagraphs and deformable mirrors are expected to enable such observations in the future. For example, Trauger and Traub (2007) have shown how contrast ratios of the order of 1×10^{-11} can be achieved with coronagraphs in the laboratory, using a laser beam at monochromatic visible wavelength. In this paper, however, a wide bandwidth is considered, in order to have enough photons in each observation. The use of a wide bandwidth in coronagraphy will require a very good achromatization of the coronagraph to achieve a high light rejection, working towards a viable visible-wavelength direct imaging technique.

2.2. Viewing Geometry

In order to simulate the observations of the Earth as if it were a distant planet, we must specify the viewing geometry of the simulated observations. An observer that looks at the Sun-Earth system from along the ecliptic will be looking at the Earth from a nearly equatorial perspective. During a year the Earth will appear to go through phases from a fully lit Earth to a fully dark Earth. For this case, the Earth would pass inside of the Sun’s glare twice per year. On the contrary an observer looking at the Sun-Earth system from a direction perpendicular to the plane of the Earth’s orbit, would see only the northern (or southern) hemisphere of the Earth. At any given time, approximately half of the Earth would be illuminated and visible to the distant observer.

In order to determine the sensitivity of our results to viewing angles, we have chosen five different viewing geometries of the Earth which we will refer to as: the equatorial view, the north/south polar view, and the (primarily) northern/southern hemisphere view. Technically, we are choosing the inclination (i) of the line of sight with respect to the ecliptic plane: 0° , $\pm 45^\circ$, and $\pm 90^\circ$. In order to visualize the viewing geometries, Figure 2 shows the Earth for a single date and time, as seen from each of the five viewing perspectives that we consider. The date corresponds to a day in November, when the Earth would present a phase angle of approximately 90° (as seen from each of our viewpoints). Note that the figure is misleading in the sense that clouds, which will play a major role in the photometric albedo, are not represented.

The quantity $p_e f_e(\beta)$ is affected by three factors. First, as the Earth’s revolves around the Sun, $p_e f_e(\beta)$ will change due to a changing β . At the same time, due to the Earth’s rotation, the portion of the Earth’s surface visible to the observer will also change, leading to changes in the albedo diurnal cycle. Finally, the large-scale cloud patterns will change from day to day, adding short-term variability to the observations. In Figure 1 the yearly

evolution of the flux ratio between the Earth and the Sun, taking into account these various effects, are represented.

We generate photometric time series of the light scattered by the planet toward an observer that include the effects of both the planet’s rotation and the planet’s orbital motion (as well as changing cloud and snow/ice cover). While our simulated data is centered on a phase angle of $\beta = 90^\circ$, the phase angle deviates from 90° due to the orbital motion (e.g., up to $\simeq 28^\circ$ for an eight week time series with the equatorial viewing geometry).

2.3. Observational Considerations

Several considerations need to be taken into account before we can realistically analyze our simulations in terms of the Earth as an exoplanet. A space telescope intending to the search for exoplanets will have a long list of target stars to observe during the planned mission life time (of order a few years). If a small number of remarkable Earth-like planet candidates are identified, then multiple months of observations time could be devoted to characterizing individual targets. On the other hand, if many Earth-like planet candidates are found, then the amount of observing time available for follow-up observations of most targets could be much more limited. Therefore, we have considered simulated observational data sets spanning 2, 4, and 8 weeks. Similarly, we have simulated observations made with several temporal resolutions (exposures times), ranging from 0.1 to 10 hours. Finally, we have added Poisson noise to the data, to simulate signal-to-noise (S/N) ratios, for each exposure time, ranging from 3 to 1000. While such a large S/N is unrealistic for a first generation TPF-C mission, these calculations are relevant for determining if very high-precision rotation measurements are possible or if the stochastic nature of clouds results in a limit on the precision of rotation periods that is independent of the S/N.

The orbital position of the planet will also limit our observing capabilities. Ideally one would like to observe the planet at full phase when its brightness, as compared to that of the parent star, is larger. However, observations at these phase angles are nearly impossible due to the small angular distance between the planet and the star. In this work, we focus on observations made near a phase angle of 90° , when the planet-star separation is near its maximum. The best case scenario for measuring the rotation period of a planet occurs for an orbital plane nearly perpendicular to the line of sight, so that the planet remains at a phase angle of nearly 90° (maximum angular separation) for it’s entire orbit orbit.

3. Results

We simulate several time series of the Earth’s scattered light towards a hypothetical observer. For each time series, we perform an autocorrelation analysis. For example, in Figure 3, the black curve shows the autocorrelation as a function of the time lag based on a simulated data series for an Earth without any cloud cover. We assume the $i = 90^\circ$ viewing geometry described in §2.2 and observations with a signal-to-noise ratio of 40 and 0.1 hour temporal resolution. Such assumptions are clearly optimistic, but not completely unreasonable. A 8m x 3.5m TPF-C mission could make such a high precision measurement for an Earth-like planet (i.e., 25 magnitudes fainter than the host star) with a 24 hour rotation period in the Alpha Centauri system (based on a 400 nm bandpass centered on 650nm, an extrasolar zodiacal light equal to that of the solar system, and the algorithm and other assumptions from “case A” of a TPF-C mission described in Brown (2005)). Therefore, if terrestrial planets are ubiquitous, then even a first generation TPF-C mission may be able to determine the rotation periods of terrestrial planets with high precision.

In §3.2 we will show that the rotation period can be measured with moderate precision using only a signal-to-noise ratio of ~ 20 every ~ 16 th of a rotation period. An 8mx3.5m TPF-C mission could achieve such photometric precision for stars brighter than $V=4$. In §5, we will further discuss the capabilities of such a TPF-C mission, as well as missions of alternative sizes. Based on the TPF Target List Database (v1; <http://sco.stsci.edu>; see also Turnbull and Tarter, 2003), we find that 29 such main sequence K-A stars that have accurate parallax, B-V color, no companion stars within $10arcsec$, and show no indications of variability. Eliminating A stars reduces the number of such targets to 15. Note that this is more than the 14 and 5 target stars included in the TPF Target List Database ‘extended’ (including A stars) and ‘core’ (excluding A stars) lists that apply several additional cuts based on a notion of habitability (e.g., eliminating young stars that may be too young for significant biological alteration of the atmosphere).

3.1. Measuring the Rotation Period

By definition, the maximum autocorrelation equals unity at zero lag. The next greatest autocorrelation occurs at 24 hours, very near the true rotation period of the Earth. In this case, we find that the amplitude of the autocorrelation is very similar at integer multiples of the Earth’s rotation period, since the only changes are due to the slow variations of the viewing geometry and phase angle (β) resulting from the orbital motion of the Earth.

For a cloudless Earth, we find that there is a second series of local maxima in the

autocorrelation function near twelve hours. This is not due to a fundamental property of the autocorrelation analysis (e.g., the blue curve for the cloudy Earth has no significant amplitude at 12 hours), but rather is due to the distribution of continents and oceans on the Earth. For this data set, the difference in the amplitude between the local maxima at 12 hours and 24 hours would indicate that the peak at 24 hours corresponds to the rotation period. However, the possibility of the continental distribution leading to a significant autocorrelation at alternative lags could complicate efforts to identify the rotation period.

We now consider a cloudy Earth using Earth’s actual cloud cover randomly selected for eight weeks in 1985. The blue curve in Figure 3 shows the results of an autocorrelation analysis similar to the one for the cloud-free Earth, assuming the same viewing geometry and observational parameters as above. Aside from the maximum at zero lag, the maximum autocorrelation occurs at 24 hours, very near the true rotation period of the Earth. The additional local maxima of the autocorrelation that occur at integer multiples of 24 hours are due to the viewing geometry repeating after multiple rotations of the Earth. In this case, the the autocorrelation decreases at larger multiples of the rotation period, since the variations in the cloud patterns are typically greater on these longer time scales.

3.2. Accuracy and Limits in the Measurements

Here, we explore how the precision of the measured rotation period depends on various observational parameters, such as the signal-to-noise ratio, the temporal resolution of observations, the total duration of the observational campaign, and the viewing geometry.

In Figure 4 (top), we show the mean absolute value of the difference between the actual and the derived rotation period of the Earth based on 21 data sets, each for a different year (Global cloud coverage measurements from ISCCP satellite observations are only available over the period 1984-2005, i.e. 21 years). Here we assume 8 weeks of observations with a temporal resolution of 6 minutes. Each curve corresponds to a different viewing geometry. For the equatorial and primarily northern/southern hemisphere views, we conclude that a S/N ratio of 10-20 is necessary to determine the rotational period with an error of about 1 hour (5% of the 24-hour rotation period). With a S/N ratio of about 30, we find a precision in the rotation determination of approximately 10 minutes (0.7%). On the other hand, the determination of the rotational period from a polar perspectives has a larger error. Even with increasing S/N, the rotational period that one obtains from a polar perspectives does not always converge to 24 hours but to a shorter periodicity (see §4.2 for further discussion).

In Figure 4 (bottom), we show the mean absolute value of the difference between the

actual and derived rotation period of the Earth, but as a function of the temporal resolution of the photometric observations. We assume a fixed signal-to-noise of 50 and an 8 week observing campaign. It is clear from the figure that a temporal sampling no larger than 1.5 hours (6% of the period) is desirable, if we want to derive the rotational period with precision. Again we find very different results for the polar viewing geometries than for the rest of viewing geometries (not shown). For the polar geometries, the integration time is not the key factor in determining the rotation.

For the equatorial view and primarily northern/southern hemisphere views, the rotation period can be determined accurately, provided that the exposure time is shorter than 1.5 hours. For exposure times larger than about 1.5 hours, the periodicity near 12 hours might be mistaken for the true rotation period.

For a general planet, we expect that the temporal resolution needed will scale with the planet’s rotation rate. E.g., a similar planet with a rotation period of 8 hours, would require that the exposure times be reduced by a factor of three to achieve a similar precision in the determination of the rotation period.

3.3. Autocorrelation vs Fourier

Here, we explore the outcome of performing a periodicity analysis to our simulated photometric time series, using a Fourier-based technique, the classical periodogram. In Figure 5 we have plotted the periodogram of the time series resulting from simulations of the real (cloudy) Earth, as viewed from the five different viewpoints and in two different years. For each case, the periodogram is calculated using time series spanning 2, 4 and 8 weeks of observations.

According to the periodogram analyses, the 24-hour periodicity is not always the strongest, and it is missing altogether for some of the series (depending on the specific cloud data). The observations from the nearly equatorial perspective seem to be the most affected by the Earth’s particular continental distribution, as there are strong peaks at 12-hours. If the distribution of continents on our planet were different (as it has been in the past), then the derived periodicities would also be different. The viewing geometry also plays a role. For example, our southern pole viewing geometry results in the Earth appearing to have a single continent in the center surrounded by ocean.

We compare the accuracy and precision of two types of periodicity analysis: the autocorrelation function and Fourier analysis. In Table 1, we show the frequency with which each type of analysis results in a determination of the rotation period near the true rotation

period ($24 \pm \Delta$ hours), half the rotation period ($12 \pm \Delta$ hours), or other alternative values. In each case $\pm \Delta$ is taken as the exposure time (or sampling resolution). In other words, a 95% value in the 24-hour periodicity for the autocorrelation method, means that for 20 of the 21 available years (cloud configurations) the primary periodicity retrieved by the autocorrelation method is $24 \pm \Delta$. In Table 2, we present the the same quantities as in Table 1, but this time for an Earth completely free of clouds, so that the detected periodicities are due to surface albedo variations only. The Fourier analysis often results in the largest peak near 12 hours (see Fig. 5), particularly for viewing geometries with orbital inclinations of 45° , 90° , and 135° . Our autocorrelation analysis never makes this error. Thus, we conclude that the autocorrelation function provides a more robust and more accurate tool for characterizing the rotation period of a planet using photometric time series data.

4. The Effect of Clouds

Clouds are common on solar system planets, and even satellites with dense atmospheres. Clouds are also inferred from observations of free-floating substellar mass objects (Ackerman and Marley, 2001). Hence, cloudiness appears to be a very common phenomenon.

Clouds on Earth are continuously forming and disappearing, covering an average of about 60% of the Earth’s surface. This feature is unique in the solar system to Earth: Some solar system planets are completely covered by clouds, while others have very few. Only the Earth has large-scale cloud patterns that partially cover the planet and change on timescales comparable to the rotational period. This is because the temperature and pressure on the Earth’s surface allow for water to change phase with relative ease from solid to liquid to gas.

In principle, weather patterns and/or the orbital motion of the Earth could pose a fundamental limitation that prevents an accurate determination of the Earth’s rotation period from the scattered light. Since the scattered light is dominated by clouds, it might be impossible to determine the rotation period if the weather patterns were completely random. Alternatively, even if the atmospheric patterns were stable over many rotation periods, observational determinations of the rotation period might not correspond to the rotation period of the planet’s surface, if the atmosphere were rotating at a very different rate (e.g., Venus).

In fact, we find that scattered light observations of the Earth could accurately identify the rotation period of the Earth’s surface. This is because large-scale time averaged cloud patterns are tied to the surface features of Earth, such as continents and ocean currents. This relatively fixed nature of clouds (illustrated in Figure 6) is the key point that would allow Earth’s rotation period to be determined from afar.

Figure 6 shows the averaged distribution of clouds over the Earth’s surface for the year 2004. The figure also shows the variability in the cloud cover during a period of two weeks and over the whole year 2004. The lifetime of large-scale cloud systems on Earth is typically of about 1-2 weeks (roughly 10 times the rotational period). In the latitude band around 60° south, there is a large stability produced by the vast, uninterrupted oceanic areas.

4.1. The Folded Light Curves

In Figure 7, we show the folded light curve of the Earth in terms of the albedo anomaly, both with and without clouds. Albedo anomaly is defined as the standard deviation (rms) from the mean value over the entire 8-week dataset (e.g., an anomaly value of 0.7 means that the albedo is 30% lower than the mean). Here we assume an exposure time of 1 hour and $S/N=30$. The real Earth presents a much more muted light curve due to the smoothing effect of clouds, but the overall albedo is higher. Note that the Y scale in the figure are anomalies and not the absolute albedo values.

In the top panels of Figure 7 data from 8 weeks of continuous observations are folded into a single light curve. In the middle and lower panels, this 8 week period is subdivided and plotted in 3 and 6 periods of 18.6 and 9.3 days, respectively. For a cloudless Earth (left panels), the error in the albedo anomaly at a given phase decreases as shorter durations are taken, because changes in phase and illuminated area decrease.

On the contrary, for the real cloudy Earth (right panels), as the data is subdivided in smaller integration periods, the size of the error bar in the albedo anomalies does not decrease, because of the random influence of clouds at short time scales. In the lower right panel of Figure 7, the light curves of consecutive 9-day integration periods vary arbitrarily in shape from one to the next.

Thus, the variability in the averaged light curve is primarily the result of short-term variability in the cloud cover, a fact that can be exploited in future exoplanet observations. Once the rotational period has been determined, one can measure the average light curve of an exoplanet, and the excess scatter for different consecutive periods. If the excess scattering does not decrease at short time periods, and the changes are not smooth in time, such an analysis can indicate the presence of clouds in its atmosphere. However, distinguishing the changes in the exoplanets light curve from the observational noise will require very stringent S/N ratios. Fortunately, there might be a better way to probe for cloudiness in an exoplanet’s atmosphere that we discuss in the following section.

4.2. Real and Apparent Rotational Period

For extrasolar planet observations, a long time series could be subdivided into several subsets. Each can be analyzed for significant periodicities as in Figure 8. The data spanning for 8 weeks is subdivided in several equal-length subperiods (e.g., six periods each of about 9 days) and analyzed independently, so that the changes in β and illumination area are minimized. In this case, several peaks appear in the Fourier periodograms and autocorrelation functions near 12 and 24-hours. The autocorrelation analysis show much greater correlation near 24 hours. For our Earth model with clouds, the best-fit rotation period shifts slightly to shorter periods. The shifts in the best-fit periodicity from the true periodicity are completely absent when considering an Earth model free of clouds for the same dates and times, even when including added noise. Therefore, we conclude that they are produced by variable cloud cover.

The shifts are introduced by the large-scale wind and cloud patterns (Houghton, 2002). Since clouds are displaced toward the west (in the same direction of the Earth’s rotation) by the equatorial trade winds (and to a minor extent by the polar easterlies) the apparent rotational period should be shorter than the rotation period of the surface. On the other hand, when clouds are moved toward the east (in the opposite direction of the Earth’s rotation) by the westerly winds at mid-latitudes, the apparent rotational period should be longer than the rotation period of the surface.

In principle, both longer and shorter periodicities could be present in the periodograms, depending on the particular weather patterns. In our models however, we often find shorter apparent rotation rates, but not longer. The explanation probably lies in the different mechanisms of cloud formation on Earth. In the tropical regions most of the clouds develop through deep convection. This deep convective clouds have a very active cycle and a short lifetime, in other words, these cloud systems do not travel far. At mid-latitudes however, deep convection does not occur, and large weather and cloud systems remain stable (and moving) for weeks (Xie, 2004).

Thus, both observing changes (anomalies) in the apparent rotational period and the amount of scatter about the phase-averaged light curve, one can recognize variable cloud cover and distinguish it from the presence of strong surface inhomogeneities, and the presence of a cloud layer. Thus, photometric observations could be used to infer the presence of a ‘variable’ surface (i.e. clouds), even in the absence of spectroscopic data. This would strongly suggest the presence of liquid water on the planet’s surface and/or in the planet’s atmosphere, especially if the mean temperature of the planet were also determined. This could be an early step in selecting the most desirable targets for more intensive follow-up and/or observations with future more advance missions with more powerful spectroscopic capabilities.

5. Implications for Future Missions

Finally, we consider the implication for future space missions. We have shown that the integrated scattered light from the Earth contains enough information to determine Earth’s rotation period. However, realistic space missions will likely be photon-starved. Here, we address whether precise measurements of the rotation period might be practical with next-generation observatories. First, we will ask for what mission specifications and target stars would it be possible to measure the rotation period of an Earth-close to $\sim 2\%$ precision. This choice is based on our simulated analysis of the Earth’s light curve that show the rotation period can be determined to an average of $\sim 2\%$ from data spanning 56 days with a signal-to-noise ratios of ~ 20 or greater and an integration times no longer than ~ 1.4 hours. Our simulations reveal a significant decrease in the precision of the measured rotation period for lower signal-to-noise ratios or longer integration times. Moreover, for extrasolar Earth-like planets, other parameters, such as the viewing geometry or the continental distribution, will play a major role in whether we will be able to measure the rotational period and with which level of accuracy. Future research should investigate whether certain wavelengths or combinations of observations can provide more robust measurement of rotation periods.

Proposed missions such as the Terrestrial Planet Finder coronagraph (TPF-C), Darwin, or SEE-COAST, are still in the planning stages and final specifications are not yet available. For the sake of concreteness, we follow Brown (2005) and consider a TPF-C mission with an $8\text{m}\times 3.5\text{m}$ primary mirror observing an Earth-like planet which is 25 magnitudes fainter than the host star (their “case A”), except that we assume an extrasolar zodiacal light that is equal to that of the solar system. We find that a signal-to-noise ratio of 20 can be obtained within 1.4 hours (for a 110nm bandwidth) for host stars of magnitude ~ 3.8 or brighter. Therefore, we estimate that there are ~ 11 such stars included in the possible TPF-C target list of Brown (2005) around which an Earth clone’s rotation period could be measured to $\sim 2\%$. If we were to scale up the primary mirror of TPF-C by a factor of two ($16\text{m}\times 7\text{m}$), then the limiting magnitude increases to $V\sim 4.4$, and there are ~ 35 stars in the sample target list of Brown (2005) for which an Earth clone’s rotation period could be measured to $\sim 2\%$. If a bandpass of $\sim 400\text{nm}$ were practical, then the limiting host star magnitude might increase by roughly one magnitude, making it possible to measure rotation periods for Earth-clones around ~ 35 or ~ 90 stars, for the two mission scenarios. We caution that these last two figures are very approximate, since the expressions of Brown (2005) break down for large fractional bandpasses.

It would be somewhat easier to achieve the needed signal-to-noise ratios for a planet that rotates more slowly than the Earth. If we were to ignore the effects of the planet revolving around the host star, then our results could be scaled to apply to an Earth-like planet with

a rotation period of P_{rot} . For such a planet, the threshold for achieving a rotation period precision of $\sim 2\%$ would require achieving signal-to-noise ratio of 20 with integration times of no more than ~ 1.4 ($P_{\text{rot}}/24$). In Figure 9, we show this threshold as a function of the rotation period and the V magnitude of the host star. The different line styles indicate the assumed major axis of the primary mirror (assuming the aspect ratio is held fixed at 16/7). For Earth-like planets above and to the right of these contours, we estimate that the rotation period could typically be measured to $\sim 2\%$ or better.

The above estimates assume that the cloud patterns on the Earth would not be affected by the alternative rotation period. Further, the above estimates also assume that the duration of the time series scales with the rotation period of the planet. A single continuous time series would be impossible for a planetary system viewed nearly edge-on, since the planet would periodically pass inside the glare of the star (or inner working angle of the coronagraph). Further research is needed to determine how well the rotation period could be measured by combining multiple shorter photometric time series, and which are the most suitable spectral ranges. For a planetary system with an orbital plane nearly in the plane of the sky, it would be possible to obtain photometric time series spanning $56 \times P_{\text{rot}}$, even for slowly rotating planets. Depending on what other planets have been found, it might or might not be practical to devote so much mission time to a single planetary system. We also caution that for planets with extremely slow rotation periods that approach the orbital period (e.g., Venus), our assumed scaling may break down due to seasonal effects and the large changes in the viewing geometry.

6. Conclusions

Exoplanets are expected to deviate widely in their physical characteristics and not all exoplanets will have photometric periodicities. Some planets, such as Venus, are 100% cloud covered and show no significant photometric variability with time. A variable photometric data set with no autocorrelation signal may be indicative of slow rotation or chaotic weather.

On Earth, the presence of continents and ocean currents results in relatively stable global cloud patterns, despite large variability on short time and length scales. Here we have shown that, despite Earth’s dynamic weather patterns, the light scattered by the Earth to a hypothetical distant observer as a function of time contains sufficient information to measure Earth’s rotation period to within a minute, on the most favorable cases. The accuracy in the rotational period determination is a function of the viewing geometry, S/N ratio, temporal sampling and the duration of our simulated time series. The rotation period could be directly compared to numerical simulations of planetary formation, to probe the

late stages of planetary accretion.

According to our calculations, the duration of the observations is comparable to the integration times needed for spectroscopic observations to search for multiple atmospheric biomarkers (Traub et al, 2006). Thus, we recommend that a photometric time series spanning weeks to months be carried out simultaneously with planet spectral characterization, via “spectrophotometry”. Photon counting CCDs have no read noise and are being adopted in mission concept studies for TPF-C and related missions (Woodgate et al, 2006). Such photon counting CCDs tag photon arrival at different wavelengths, and allows later binning in different ways. Observations of an exoplanet spanning several weeks could be binned over the entire observational period to retrieve a low-resolution spectra and characterize its atmospheric composition. Additionally, the data could also be binned in shorter time periods over all wavelengths in order to retrieve the rotation rate and explore the presence of active weather.

We have shown in this paper that, if the rotation period of an Earth-like planet can be determined accurately, one can then fold the photometric light curves at the rotation period to study regional properties of the planet’s surface and/or atmosphere. Most significantly we could learn if dynamic weather is present on an Earth-like exoplanet, from deviations from a fixed phase curve. In contrast, a cloud-free planet with continents and oceans would not show such light curve deviations. With phased light curves we could study local surface or atmospheric properties with follow-up photometry, spectroscopy, and polarimetry, to detect surface and atmospheric inhomogeneities and to improve the sensitivity to localized biomarkers. Finally, we have also provided guidance for the necessary specifications for future space missions.

Research by E. Pallé was supported by a ‘Ramon y Cajal’ fellowship. Support for E.B. Ford was provided by NASA through Hubble Fellowship grant HST-HF-01195.01A awarded by the Space Telescope Science Institute, which is operated by the Association of Universities for Research in Astronomy, Inc., for NASA, under contract NAS 5-26555.

REFERENCES

- Ackerman, A.S., Marley, M.S. 2001, *The Astrophysical Journal* 556, 2, 872-884
- Agnor, C.B., Canup, R.M., Levison, H. F. 1999, *Icarus*, 142, 219
- Brown, R. 2005, *The Astrophysical Journal* 624, 1010

- Bushby, P., Mason J. 2004, *Astronomy & Geophysics* 45, 4, 4.07-4.13
- Cash, W. 2005, *Nature*, 442, 51
- Chambers, J. E. 2001, *Icarus*, 152, 2, 205-224
- Ford, E.B., Seager, S., Turner, E.L. 2003, *Nature*, 412, 885-887
- Fridlung, M.C. 2004, *Proceedings of SPIE*, 5491
- Gaidos, E., Williams, D.M. 2004, *New Astronomy* 10, 1, 67-77
- Gelino, C., Marley, M. 2000, *ASP Conference Series* 212, C.A. Griffith and M.S. Marley (eds)
- Goldreich, P., Lithwick, Y., Sari, R. 2004, *ApJ*, 614, 497
- Grießmeier, J.-M. 2007, *Planet. Space Sci.*, 55, 530
- Houghton, J. 2002, *The Physics of Atmospheres*, Cambridge University Press
- Kaltenegger, L., Traub, W.A., Jucks, K.W. 2007, *Astrophysical Journal*, 658, 598-616
- Kaltenegger, L. 2005, *Search for Extra-Terrestrial planets: The DARWIN mission - Target Stars and Array Architectures*, PhD. Thesis
- Laskar, J., Correia, A.C.M. 2004, *ASP Conference Proceedings* 321, J. Beaulieu, A. Lecavelier and C. Terquem (eds)
- Lindensmith, C. 2003, *Bulletin of the American Astronomical Society*, 35, N.41.14
- Mawet, D., Riaud, P., Baudrand, J., Baudoz, P., Boccaletti, A., Dupuis, O., & Rouan, D. 2006, *A&A*, 448, 801
- Montañés-Rodríguez, P., E. Pallé, P.R. Goode, J. Hickey, and S.E. Koonin 2005, *The Astrophysical Journal*, 629, 1175-1182
- Montanes-Rodriguez, P., Pallé, E., Goode, P.R., Martin-Torres, F.J. 2006, *The Astrophysical Journal*, 651, 544-552
- Pallé, E., et al. 2003. *J. Geophys. Res.*, 108(D22), 4710,
- Pallé, E., P.R. Goode, P. Montañés-Rodríguez, and S.E. Koonin 2004, *Science*, 304, 1299-1301

- Rivera, E.J., Lissauer, J.J., Butler, R.P., Marcy, G.W., Vogt, S.S., Fischer, D.A., Brown, T.M., Laughlin, G., Henry, G.W. 2006, *Bulletin of the American Astronomical Society*, 37, 1487
- Rossow, W.B., A.W. Walker, D.E. Beuschel, and M.D. Roiter, 1996, *International Satellite Cloud Climatology Project (ISCCP) Documentation of New Cloud Datasets*. WMO/TD-No. 737, World Meteorological Organization, 115 pp.
- Russell, C. T. 2006, *Advances in Space Research*, 37, 1467
- Sagan, C., W.R. Thompson, R. Carlson, D. Gurnett, and C. Hord, 1993, *Nature*, 365, 715-721
- Schlichting, H.E., Sari, R. 2007, *The Astrophysical Journal*, 658, 1, 593-597
- Schneider, J., Riaud, P., Tinetti, G., and See-Coast Team 2006, *European Planetary Science Congress*, p 251
- Seager, S., Turner, E.L., Schafer, J., Ford, E.B. 2005, *Astrobiology*, 5, 372-390
- Stam, D.M., de Rooij, W.A., Cornet, G., Hovenier, J.W. 2006, *Astronomy and Astrophysics* 452, 669-683
- Suttles, J.T., R.N. Green, P. Minnis, G.L. Smith, W.G. Staylor, B.A. Wielicki, I.J. Walker, V.R. Young, and L.L. Stowe 1988, *Angular Radiation Models for Earth-Atmosphere Systems*, vol. 1, *Shortwave Radiation*, Ref. Publ. RP-1184, 26 pp., NASA, Hampton, Va.
- Tinetti, G., et al. 2006. *Astrobiology*, 6, 1, 34-47.
- Traub, W. A., et al. 2006, *Proc. SPIE*, 6268
- Trauger, J.T., Traub, W.A. 2007, *Nature*, 446, 771-773
- Turnbull, M., and J. Tarter 2003, *The Astrophysical Journal*, 149, 423
- Udry S., Bonfils X., Delfosse X., Forveille T., Mayor M., Perrier C., Bouchy F., Lovis C., Pepe F., Queloz D., and Bertaux J.-L. 2007, *Astron. & Astrophys.* , 469 , 43
- Vallee, J.P. 1998, *Fundamentals of Cosmic Physics* 19, 319-422
- Williams, D.M., Gaidos, E. 2007, *Icarus*, (submitted)
- Woodgate, B., E. Mentzell, G. Hilton, and D. Lindler 2006, *New Astronomy Review* 50, 297-300

Xie, S. 2004, BAMS, 195

Table 1: The existence of 21 years of global cloud observations allow us to simulate the photometric time series of Earth for each of these years, with the exact same geometrical configurations, with only clouds changing. For each year we have calculated the main periodicities resulting from the photometric simulations analysis. In the table, we show the percentage of years in which the main periodicity is found to be (i) $24 \pm \Delta$ hours, (ii) $12 \pm \Delta$ hours or (iii) other periods. For example a 95% value in a given periodicity, means that for 20 of the 21 available years (cloud configurations) that was the primary periodicity. Fourier and autocorrelation analysis results are both shown. In all cases $\pm\Delta$ is taken as the exposure time.

Area	24	12	other	24	12	other
	Fourier			Auto		
	S/N=20, Exp=0.5h, Followup=2w					
N. Pole	38	4	58	100	0	0
Lat +45	9	76	15	100	0	0
Equator	0	71	29	100	0	0
Lat -45	4	57	39	100	0	0
S. Pole	9	23	68	100	0	0
	S/N=20, Exp=0.5h, Followup=8w					
N. Pole	66	4	30	100	0	0
Lat +45	4	71	25	100	0	0
Equator	0	80	20	100	0	0
Lat -45	0	76	24	100	0	0
S. Pole	23	42	35	100	0	0
	S/N=5, Exp=0.5h, Followup=2w					
N. Pole	4	0	96	33	0	67
Lat +45	0	9	91	52	0	48
Equator	0	33	67	76	0	24
Lat -45	0	28	72	80	0	20
S. Pole	0	0	100	23	0	77
	S/N=20, Exp=1.7h, Followup=2w					
N. Pole	85	4	11	80	0	20
Lat +45	66	28	6	85	0	15
Equator	38	47	15	85	0	15
Lat -45	57	33	10	90	0	10
S. Pole	71	9	20	80	0	20

Table 2: Same as Table 1, but the calculations are done for a cloud-free Earth.

Area	24	12	other	24	12	other
	Fourier			Auto		
	S/N=20, Exp=0.5h, Followup=2w					
N. Pole	95	4	1	100	0	0
Lat +45	19	80	1	100	0	0
Equator	4	95	1	100	0	0
Lat -45	4	95	1	100	0	0
S. Pole	0	100	0	100	0	0
	S/N=20, Exp=0.5h, Followup=8w					
N. Pole	95	4	1	0	0	100
Lat +45	4	95	1	4	0	96
Equator	0	100	0	100	0	0
Lat -45	4	95	1	100	0	0
S. Pole	0	100	0	95	0	5
	S/N=5, Exp=0.5h, Followup=2w					
N. Pole	52	0	48	100	0	0
Lat +45	28	71	1	100	0	0
Equator	4	95	1	100	0	0
Lat -45	4	95	1	100	0	0
S. Pole	0	95	5	100	0	0
	S/N=20, Exp=1.7h, Followup=2w					
N. Pole	100	0	0	100	0	0
Lat +45	100	0	0	100	0	0
Equator	4	95	1	100	0	0
Lat -45	9	90	1	100	0	0
S. Pole	76	23	1	100	0	0

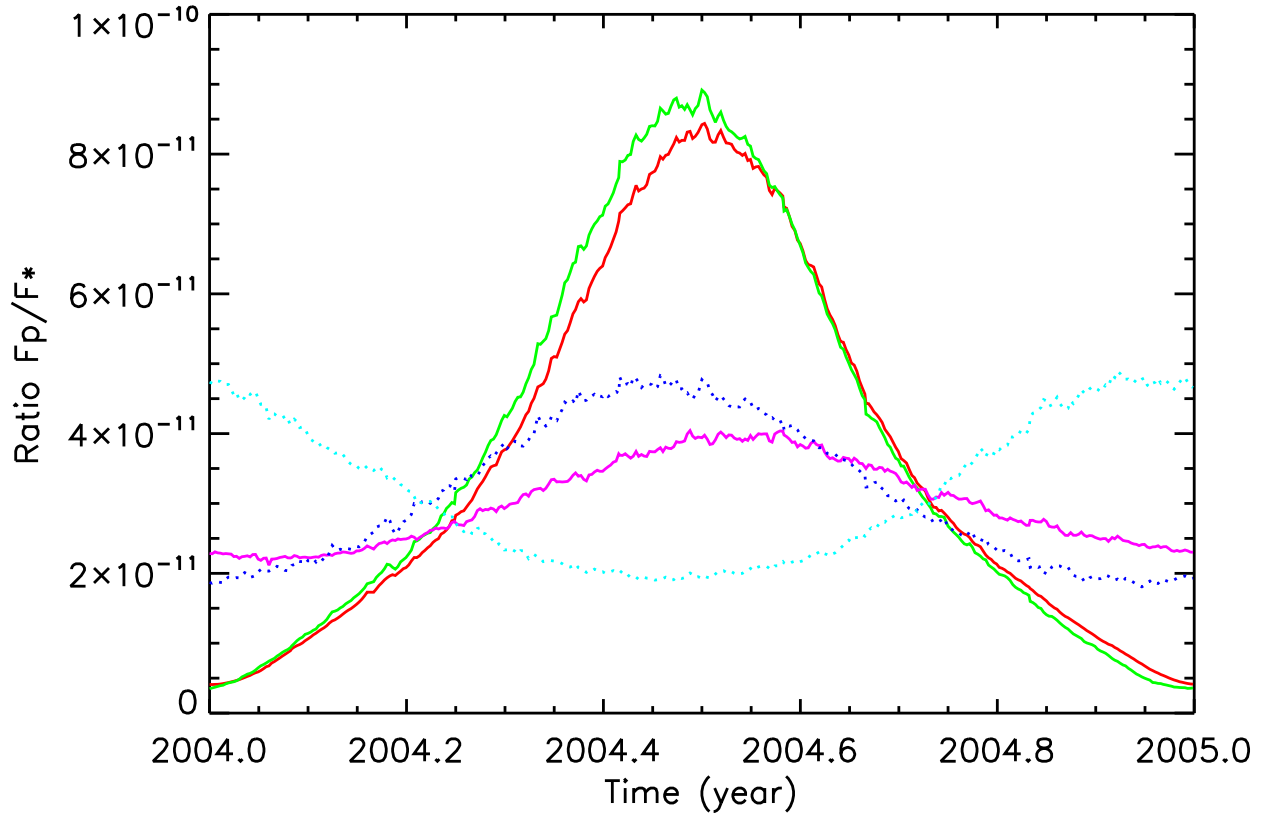


Fig. 1.— The yearly evolution of relative flux of the Earth with respect to the Sun from five different viewing geometries. The equatorial view is marked in red, the primarily northern/southern hemisphere views are in green and pink (respectively) and the north and south polar views are in dark and light blue (respectively).

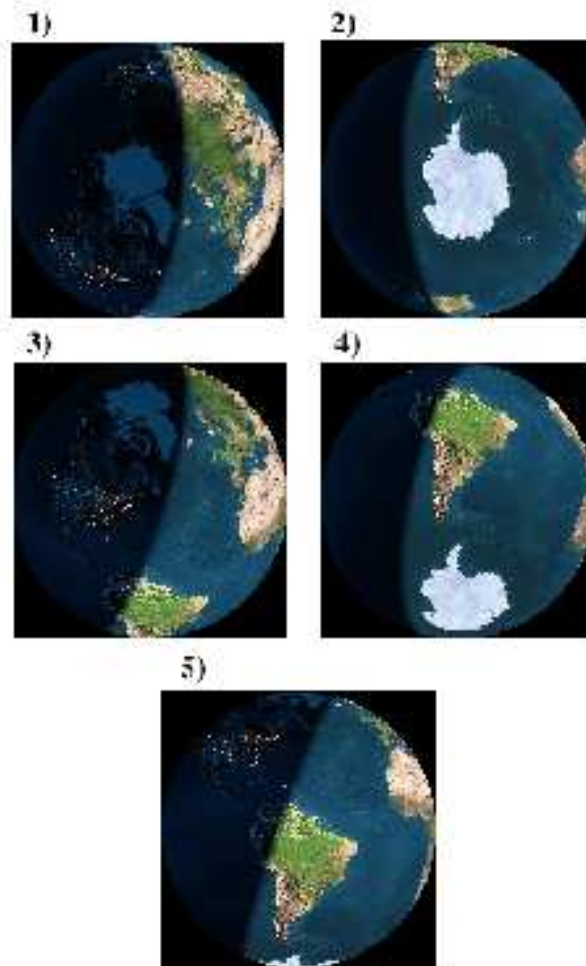


Fig. 2.— The Earth from space. The several images shown the viewing geometry of Earth for the exact same day and time (2003/11/19 at 10:00 UT) but from our five different viewpoints: from 90° above the ecliptic (north polar view) (1), from 90° below the ecliptic (south polar view) (2), from $+45^\circ$ north of the ecliptic (primarily northern hemisphere in view) (3), from -45° below the ecliptic (primarily southern hemisphere in view) (4), and from within the ecliptic (5). Note how the scenery from the different viewpoints, could well have been taken from different planets.

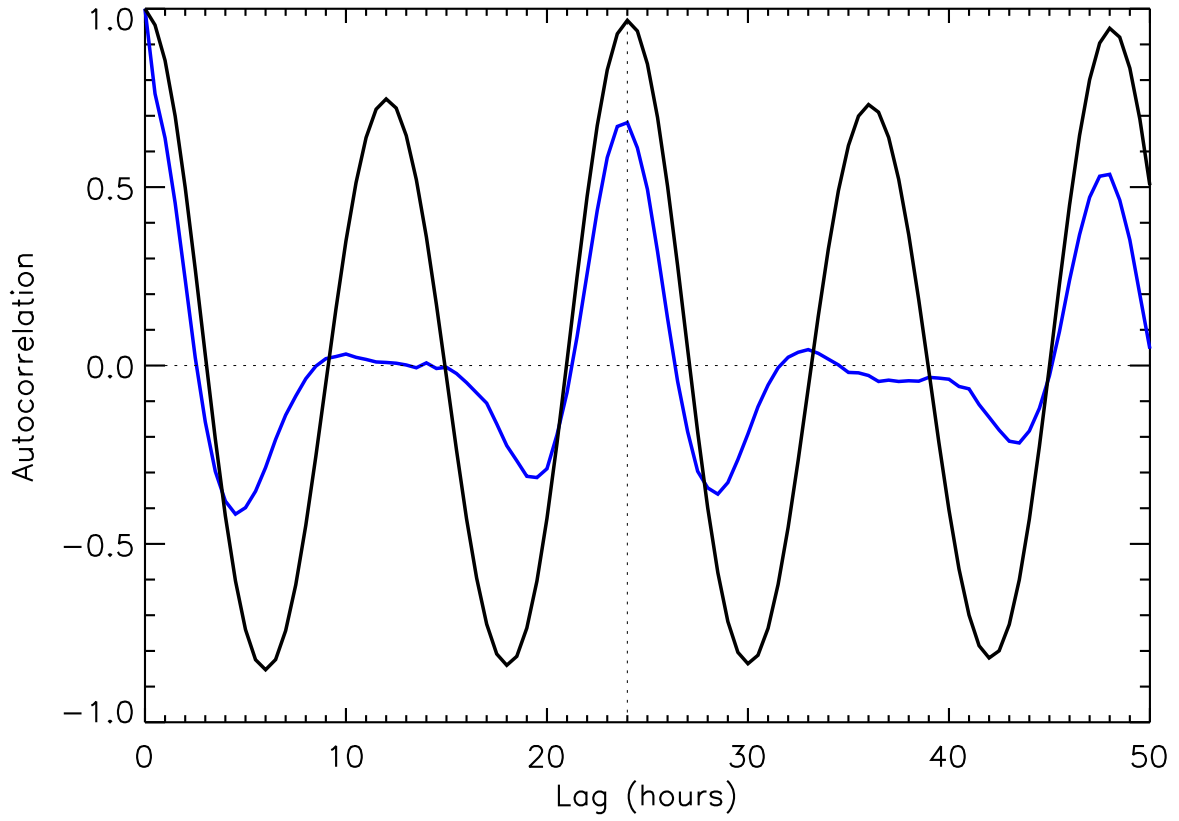


Fig. 3.— Autocorrelation function of the scattered light by the real Earth (blue) and a cloud-free Earth (black). An 8-week time series with S/N ratio of 40 and 0.1 hour observing cadence has been chosen, using cloud data from 1985.

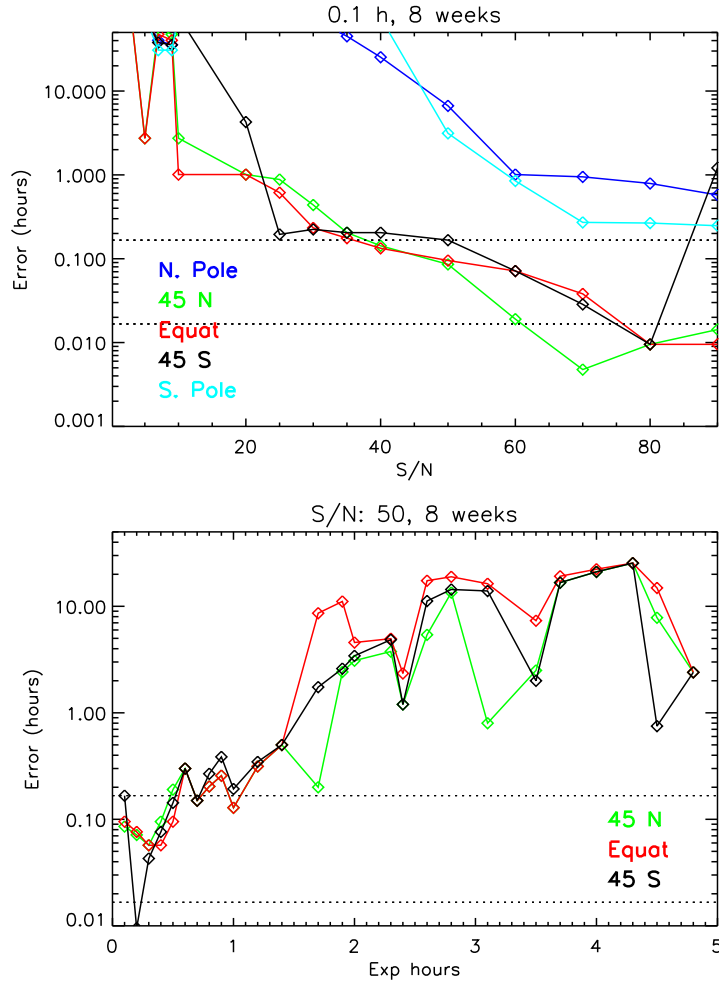


Fig. 4.— Top panel: The plot represents the error that one would get in estimating the Earth’s rotation rate from the globally integrated photometric light curve. Each point is the error of the averaged rotational period found for 21 years with different (real) cloud patterns for the same geometries. The five different colors indicate five different viewing angles (i.e. equator means the observer is looking at the Sun-Earth system from the ecliptic plane, the North pole indicates the observer is looking at the Sun-Earth system from 90° above the ecliptic). All calculations are given for a 90° phase angle in the orbit (i.e. one would see a quarter of the Earth’s surface illuminated). In the plot, the top broken line represents an accuracy in determining the rotational period of 10 *minutes*, and the lower one of 1 *minute*. Lower panel: Same as in the top panel, but this time the S/N is fixed and the exposure time is allowed to vary. As in the top panel, an object follow up of two months (8 weeks) is considered.

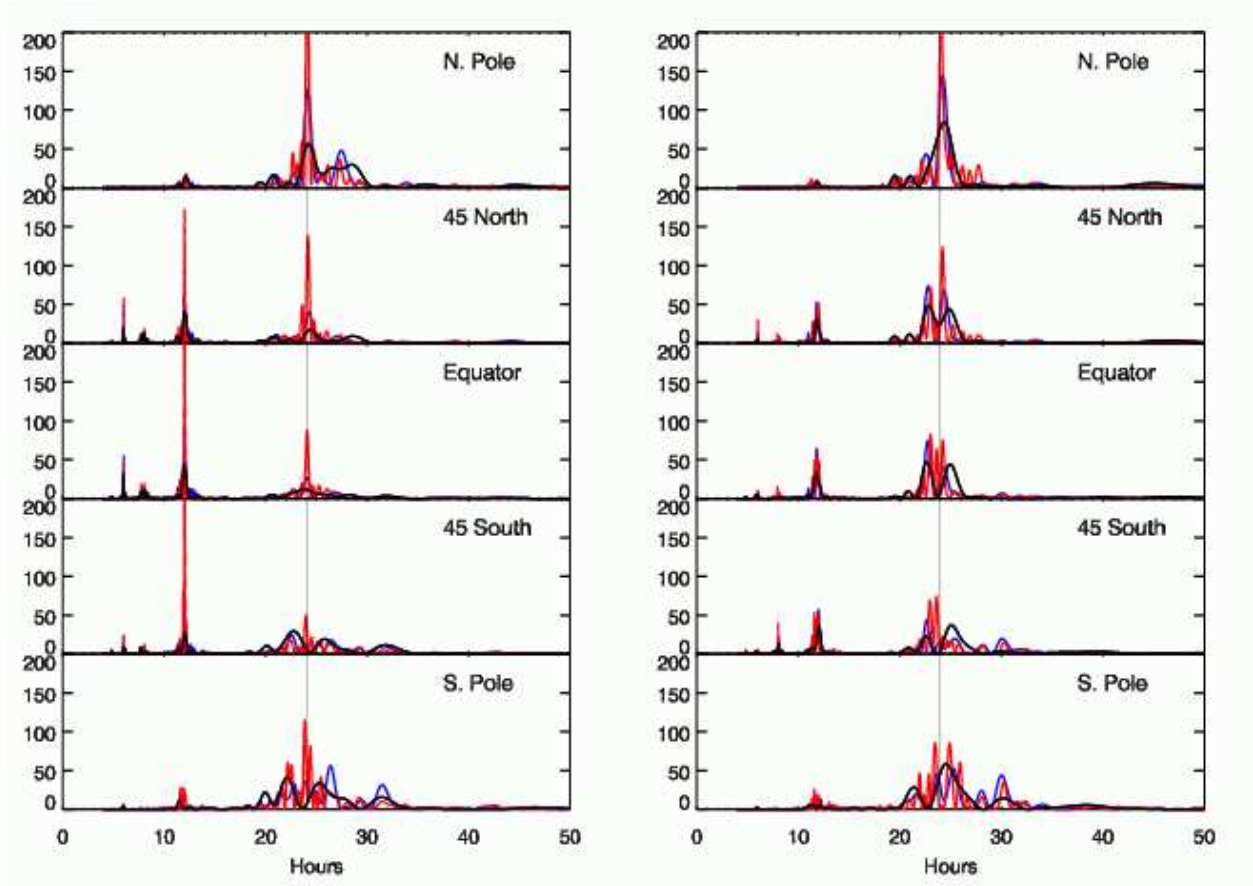
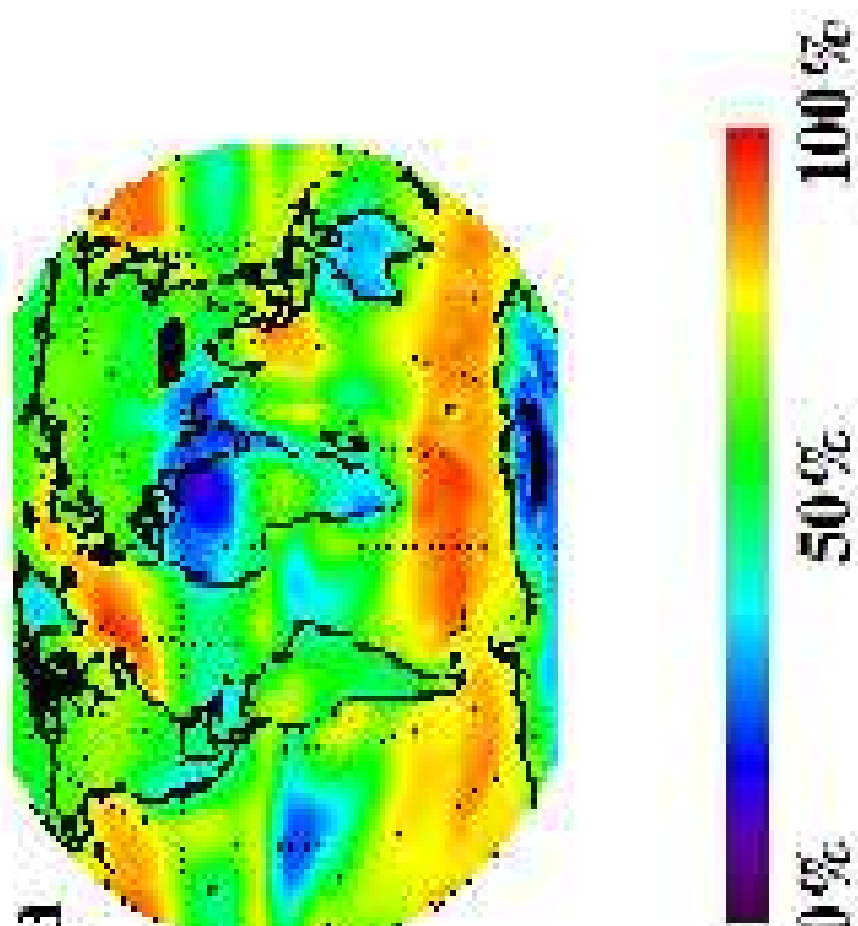
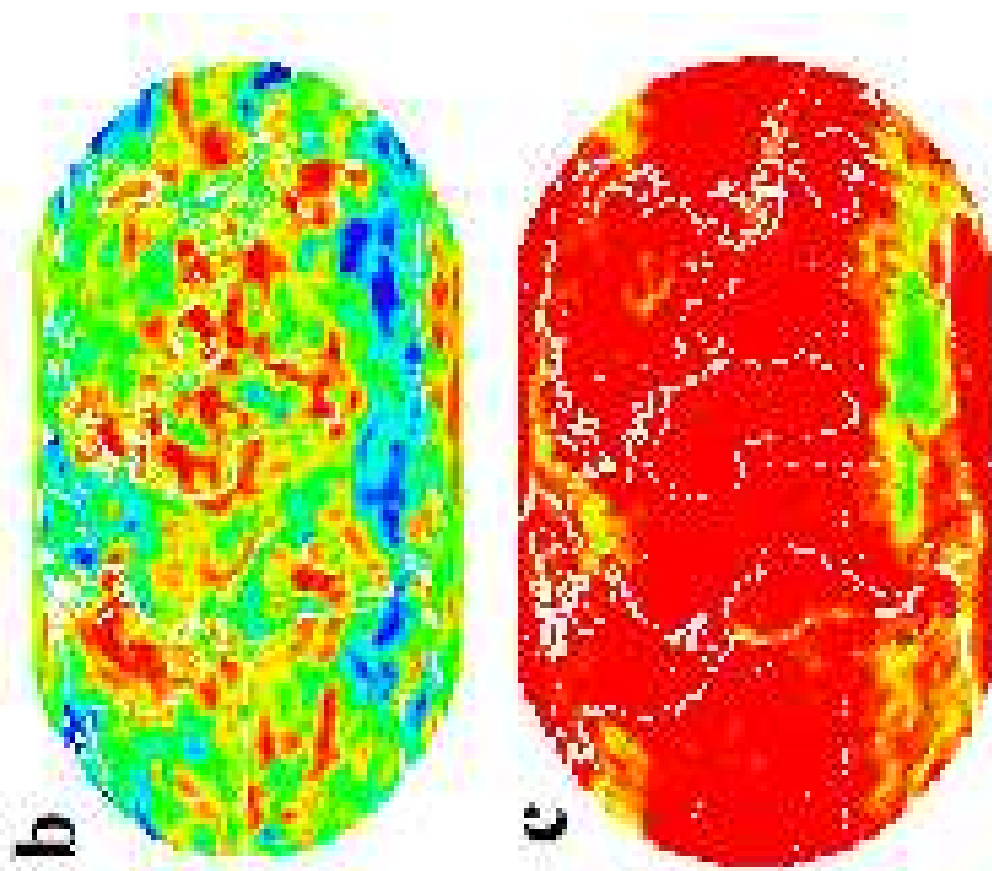


Fig. 5.— Periodogram analysis of the Earth’s $p_e f_e(\beta)$ times series as seen from five different viewpoints, at phase angle 90° . From top to bottom, the five viewpoints are: the north polar view (a), primarily northern hemisphere view (b), the equatorial view (c), primarily southern hemisphere view (d), and the south polar view (e). The right column represents the periodograms for the year 2000, while the left column represents the periodograms for year 2004. The geometry is exactly the same for the two years, only the clouds have changed. In all panels, the periodogram is shown for data lasting for a period of 2 (black line), 4 (blue line) and 8 weeks (red line) around phase 90° . In all panels a thin vertical line indicates the “real” 24-hour periodicity.



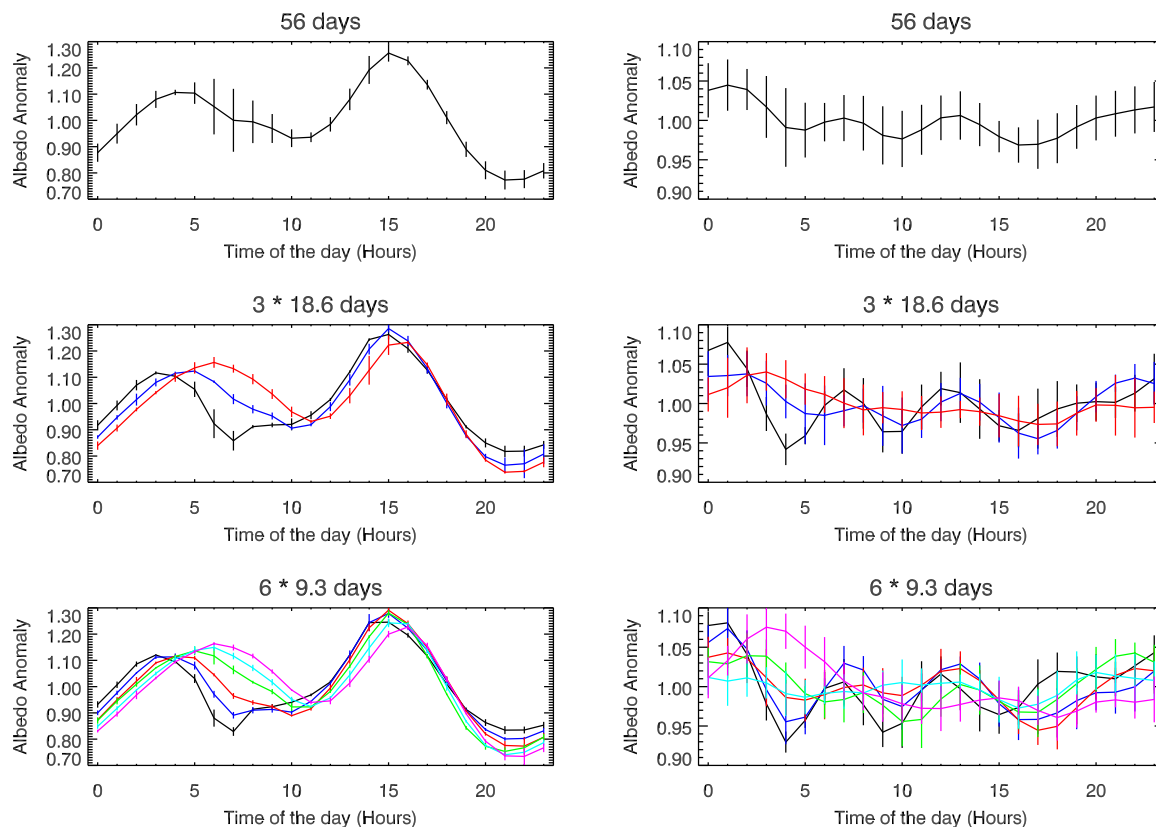


Fig. 7.— Light curves of the Earth observed from the ecliptic plane at phase 90° (half phase). Left column are the light curves of a cloud-free Earth and right columns are the light curves for the real Earth. The Y-scale in the right and left panels is different because of the more muted variability in the albedo introduced in the real Earth by clouds. Fifty six days (two months) of continuous observations are divided from top to bottom in 1, 3, and 6 sub-series, and folded over the 24-hour rotational period of the Earth for analysis. Note the contrast between the uniformity of the light curves of an ideal (cloudless) Earth and the real Earth light curves. Also note how the change in the shape of the light curve is smooth (ordered in time) from one series to the next in the case of a cloudless Earth, but it is random for the real Earth. The size of the error bars are the standard deviation of the mean.

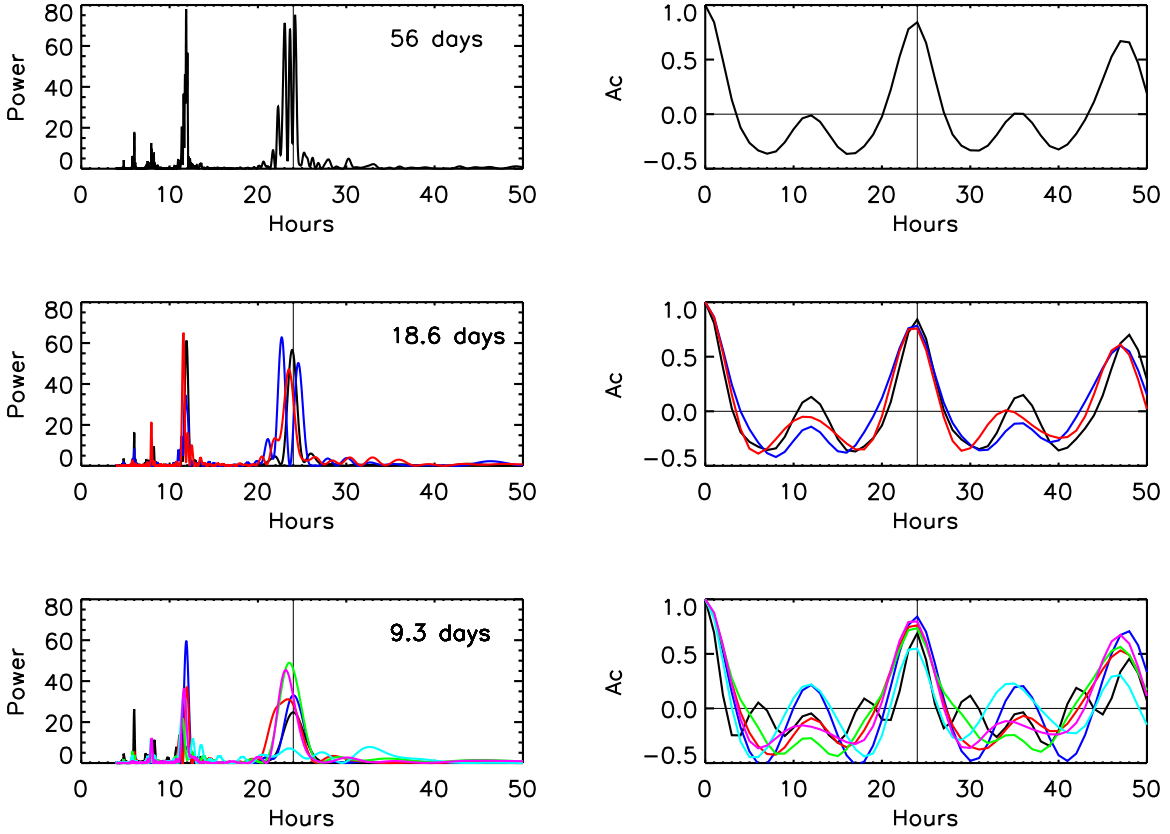


Fig. 8.— Left: Periodogram analysis of the Earth’s $p_e f_e(\beta)$ equatorial time series. Right: Autocorrelation function of the same time series. For this figure we select 8 weeks of data (56 days) and calculate the periodograms and autocorrelation functions (top panels). S/N ratio are set here to 50 for clarity purposes. Then we subdivide these data in three (middle panels) and six (bottom panels) equally-long time series and we again calculate the separate periodograms and autocorrelations. In the figures, different colors indicate different data subperiods. Note the appreciable decrease in the retrieved rotation rate for some of the time series in the bottom panels, detectable with both autocorrelation and Fourier analysis.

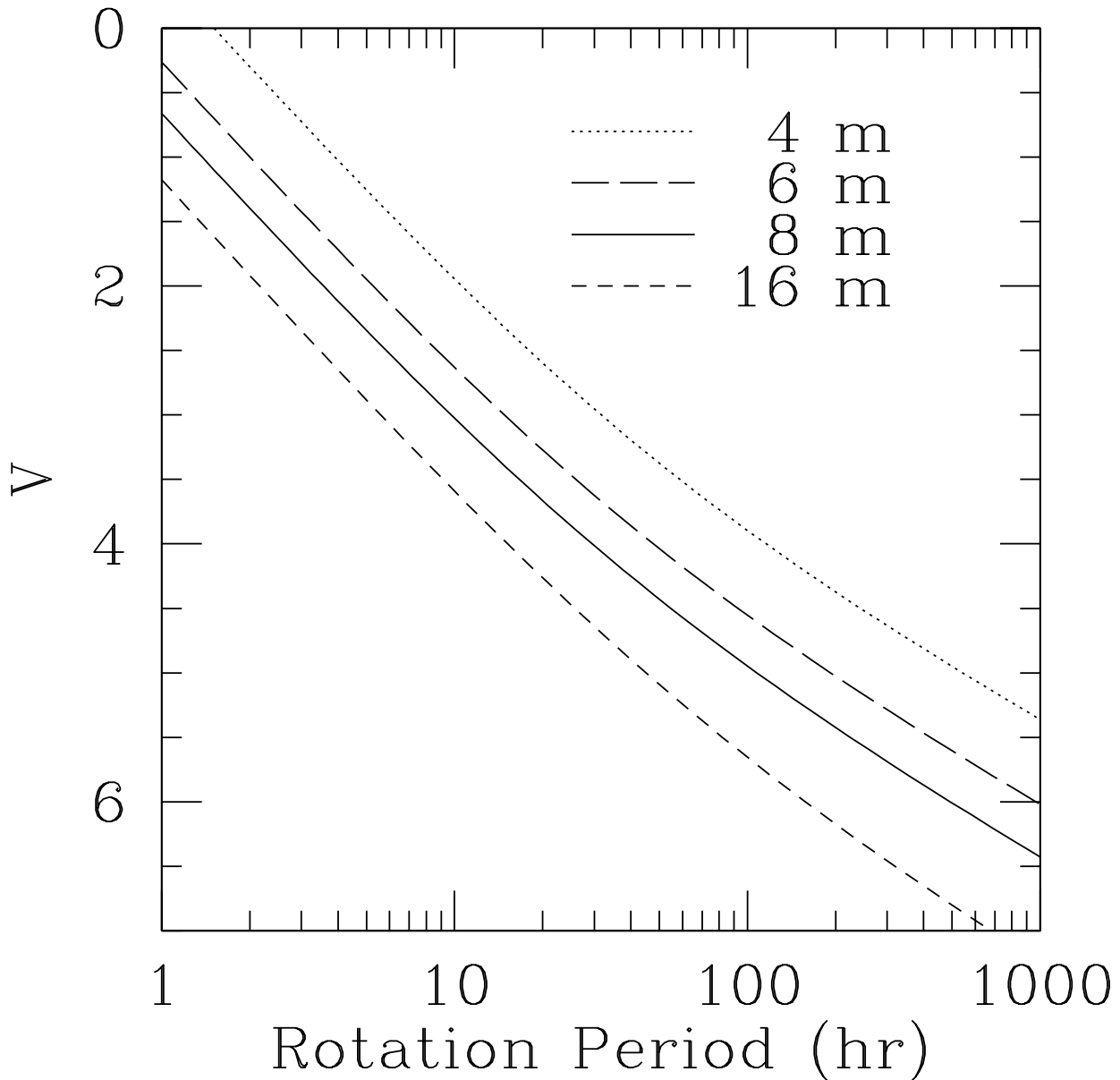


Fig. 9.— Here we show the threshold host star magnitude and planet rotation period for which a signal-to-noise of ~ 20 or greater can be obtained for each integration of ~ 1.4 ($P_{\text{rot}}/24$). Along this curve, our simulations suggest that a times series spanning $56 \times P_{\text{rot}}$ would typically result in measuring the rotation period to $\sim 2\%$ for an Earth-like planet. Higher precision measurements of the rotation period would be obtained for V and P_{rot} to the upper right of the curves. The solid curve assumes mission specifications similar to “case A” of Brown (2005), an Earth-like planet that is 25 magnitudes fainter than the host star, and an exozodi comparable to that of the solar system. The other curves assume similar mission specifications, but scale the major axis of the primary mirror to 4m (dotted), 6m (long dashed), or 16m (short dashed) and hold the axis ratio constant.